ОБЪЕДИНЕННЫЙ
ИНСТИТУТ
ЯДЕРНЫХ
ИССЛЕДОВАНИЙ

Дубна

E4-95-408

S.N.Ershov, F.A.Gareev, H.Lenske*

# ELASTIC SCATTERING OF HALO NUCLEI ON PROTONS

Submitted to «Physics Letters B»

*Institut für Theoretische Physik, Universität Giessen, Germany

1995

# 1 Introduction

Investigations of light nuclei at the neutron drip line open the possibility to study nuclear structure and reaction dynamics under the extreme conditions of large charge asymmetry. Isospin dependent effects and contributions from residual interactions are strongly enhanced. Clear indications of the unsual nuclear properties at the neutron and proton driplines have been observed in measurements of total and interaction cross sections, electromagnetic dissociation and fragmentation processes of exotic nuclei. The experiments led to the discovery of "neutron halo" in $^{11}Li$, $^{11}Be$, $^{14}Be$ [1, 2]. In a recent experiment at GSI, a proton halo was observed for the first time in $^{8}B$ [4].

A closer understanding of such extreme nuclear matter configurations is obtained from elastic and quasi–elastic scattering of exotic nuclei. These reactions are well suited to investigate the peculiarities in structure and interactions of halo nuclei. Because of their semi–inclusive character quasi–elastic processes are especially sensitive to the structure of the interacting nuclei. The underlying reaction mechanism is in principle known and the theoretical uncertainties are less severe than for exclusive reactions where correlations of various fragments are measured.

Elastic scattering has the largest cross section amongst the quasi–elastic processes and is easily accessible in secondary radioactive beam experiments with low intensity. At present, elastic scattering data are available for $^{11}Li$ on $^{12}C$ at energy 60 MeV/A [3], on $^{28}Si$ at 29 MeV/A [5] and on a proton target at 62 MeV/A [6]. Also the elastic scattering of $^{8}He + p$ was measured at the energy 73 MeV/A [7]. The cross sections were smaller than expected from the systematics of stable isotopes. This common feature of halo nuclei is associated with break-up processes. The poor energy resolution of radioactive beams leads to particular problems in the analysis of ion-ion scattering data because low lying inelastic target and projectile excitations are not resolved from pure elastic process.

Elastic nucleus-nucleon data are free from this drawback. Theoretically, the reaction mechanism of nucleon scattering is much simpler and better understood than for ion-ion interactions. Hence, elastic scattering on nucleons is most appropriate to clarify the interaction dynamics of halo nuclei. In this work, we present a reaction model for the elastic scattering of $^{11}Li$ on a proton target and try to elucidate the role of halo particles in the scattering process. The weak coupling model and the special properties of halo nuclei allows to treat the core and valence parts in different ways. The proton–core interactions are determined by same type of processes as in optical potentials for elastic scattering on stable nuclei. In the present context, this part of the dynamics is of less interest. Therefore, we treat the proton–core interaction in a schematic approach by using phenomenological optical potentials. As discussed in sect. 2, the contributions from the halo nucleons, however, are calculated microscopically in a folding model approach. Applications to $^{11}Li + p$ elastic scattering are presented in sect. 3. The results clearly indicate that the lowest order approximation obtained from a folding model is unable to account for the diffraction structure observed in $^{11}Li + p$ elastic data at $E_p = 60\ MeV$. The agreement is improved when polarization contributions are included. A new approach is presented which allows to calculate polarization potentials from weakly bound valence particles in a semi–microscopic way.



# 2 The Reaction and Structure Model

In a first approximation, halo nuclei can be considered as consisting of two almost separable and independent subsystems: the core and the weakly bound valence nucleons. A prominent case is $^{11}Li$ where two loosely bound halo neutrons are coupled weakly to a $^{9}Li$ core. It is reasonable to assume that elastic scattering occurs almost independently on both subsystems. Accordingly, the optical potential $U(r)$ for halo systems like $^{11}Li$ can be expressed as

$$U(r) = U_{core}(r) + U_{val}(r). \qquad (1)$$

where $U_{core}$ and $U_{val}$ describe the interaction with the core and the valence halo neutrons, respectively.

The microscopic derivation of the full optical potential is hampered by the complexities of many-body reaction calculations. The specific properties of dripline nuclei, however, allow to treat the the core and valence interactions separately. Therefore, we decide to use a simpler approach which is physically transparent and specifically emphasizes the dynamical contributions from the halo particles. We approximate the $^{9}Li + p$ core potential by the optical potential from the elastic scattering of a free $^{9}Li$ nucleus on a proton. Thus, the bulk of the $^{11}Li + p$ interaction is treated empirically. The approach has obviously the advantage that the full complexity of many–body effects in the proton–core subsystem is effectively included. Implicit to such a model is the assumption that the structure of the core remains essentially the same as for the corresponding free nucleus. For nuclei like $^{11}Li$ with a small number of valence particles this condition is likely to be fulfilled.

The proton–halo interactions, which are of main interest, are treated microscopically. The halo wave functions are taken from a full–scale nuclear structure calculation for the total core–plus–halo system [4, 12, 13]. A mean–field of Wood–Saxon shape with parameters taken from the systematics of stable nuclei was used. Pairing correlations were included microscopically by solving the Gorkov equations [12, 13, 14]. The particle-particle interaction in the singlet–even channel was obtained from a G-matrix. At vanishing nuclear density the free space $NN$–scattering length, $a_{NN} = -17.8\ fm$ is reproduced. The one–body density $\rho_{val}(r)$ of the valence particles is obtained from the microscopic single particle wave functions. Binding is obtained by a peculiar interplay of mean–field dynamics and residual pair interactions [4, 12, 13]

The proton–halo potential is derived by folding the microscopic valence density

distribution with a free $NN$ t-matrix interaction

$$U_{val}(r) = \int d^3r' \rho_{val}(\vec{r}') t_{NN}(|\vec{r} - \vec{r}'|) \quad (2)$$

and $U_{val} = U_{val}^{(re)} + iU_{val}^{(im)}$ includes a real and an imaginary part because $t_{NN}$ is a non-hermitian operator. From the definition of $t_{NN}$ it is clear that $U_{val}^{(im)}$ describes the complete summation over energy–conserving intermediate scattering processes between the incoming proton and a halo nucleon. Because of the weak binding of the valence particle these interactions should be in first approximation the same as for a pair of nucleons in free space.

The fact that $^{11}Li$ is particle stable although neither $^{10}Li$ nor the free two neutron system are bound indicates that nuclear structure is providing important contributions. The whole variety of such effects is globally described by a state, i.e. energy dependent, self–energy $\Sigma_{val}(\epsilon_1)$ for a valence particles with energy $\epsilon_1$. Accordingly, the intermediate propagators entering in the definition of $t_{NN}$ should be modified. Denoting by $G^*_{NN}$ and $G_{NN}$ the 2–particle propagators with and without the nuclear self–energies, we define a medium–corrected $NN$ t–matrix interaction which obeys the modified Lippmann–Schwinger equation

$$t^*_{NN} = t_{NN} - t_{NN}\,(G_{NN} - G^*_{NN})\,t^*_{NN} \quad . \quad (3)$$

Asymptotically, $G^*_{NN}$ approaches $G_{NN}$ such that in free space $t^*_{NN} = t_{NN}$. $G^*_{NN}$ also differs from $G_{NN}$ by the fact that states which are occupied by target nucleons are projected out and to do contribute to the scattering series.

The microscopic calculation of $t^*_{NN}$ is beyond the scope of the present work. Instead, we apply a more schematic but physically resonable approach. In Eq.(3) the difference of Green functions is replaced by

$$t_{NN}(G_{NN}(E) - G^*_{NN}(E))t^*_{NN} = t_{NN}|0\rangle\beta\langle 0|t^*_{NN} \quad (4)$$

where $|0\rangle\langle 0|$ denotes the projector onto the ground state and an integration over the incident particle coordinates is implicit. An effective polarization coefficient $\beta$ was introduced which describes globally the medium–dependent corrections to free $NN$ scattering. With respect to the free propagator the energy scale in $G^*_{NN}$ is shifted by the static parts of the bound and continuum potentials. This contribution will be neglected because it mainly redefines the energy scale. A more important effect – especially in dripline nuclei – is that the spectral strength is redistributed. This is connected with a renormalization of wave functions [14]. Neglecting the contributions from the incident continuum nucleon one finds in first approximation $G^*_{NN} \simeq Z^2_{val} G_{NN}$ where

$$Z^2_{val} = \frac{1}{1 - \partial\Sigma_{val}|0/\partial\epsilon_1} \quad (5)$$

is determined by the energy–dependent parts of the valence binding interactions [15, 16]. Eq.(4) is finally derived by approximating $G_{NN}$ in terms of the level density



$\rho^{free}_{val}$ for a non–interacting valence particle at $\epsilon_1 = 0$. From the relation

$$\beta = (1 - Z^2_{val})\rho^{free}_{val} \quad (6)$$

$\beta$ is seen to describe the valence level density which is effectively available for intermediate scattering processes in $t^*_{NN}$. In a stable nucleus with a sharp Fermi–surface one has $Z^2_{val} \simeq 1$ and $\beta$ is negligibly small. In soft systems like dripline nuclei which are easily polarized $\beta$ will be non–vanishing and corrections to the bare impulse approximation potential have to be expected. Theoretically, $\beta$ could be obtained from nuclear structure calculations including dynamical polarization, e.g. refs. [4, 15, 16]. At the present stage of our understanding of nuclear structure at the dripline it is justified to treat $\beta$ as a phenomenological parameter. The medium–corrected valence potential is obtained

$$U^{pol}_{val} = \langle 0|t^*_{NN}|0\rangle = \frac{1}{1 + \beta(E)\langle 0|t_{NN}|0\rangle}\langle 0|t_{NN}|0\rangle \quad . \quad (7)$$

For $\beta \to 0$ the bare valence potential $U_{val} = \langle 0|t_{NN}|0\rangle$ , Eq.(2), is recovered. Insight into the polarization contributions is obtained by expanding Eq.(7) up to first order in $\beta$ which corresponds to a correction of second order in the bare valence potential,

$$U^{(2)pol}_{val} = \beta U val^2 = \beta(U^{(im)2}_{val} - U^{(re)2}_{val} - 2iU^{(re)}_{val}U^{(im)}_{val}) \quad (8)$$

Since the bare potentials are entering quadratically $U^{pol}$ decreases more rapidly than the bulk potentials. Such a behaviour should be expected because nuclear polarization is most effective in the surface region. For standard forms of $U^{re,im}$ and positive $\beta$ the imaginary part of $U^{pol}$ carries in total a negative sign and thus increases the absorption. Physically, this is reasonable because polarization self–energies are providing additional attraction in the low energy part of nuclear spectra as found in nuclear structure calculations [15] and also from the analysis of low energy neutron scattering [17]. As a result, polarization tends to increase the level density close to particle threshold. This has important consequences for absorptive processes because the energy gap for the scattering of the valence particles into intermediate states is effectively decreased.

## 3 Applications to p+$^{11}$Li elastic scattering

The model has been applied to elastic scattering of $^{9,11}Li$ on a proton target at an incident energy $E/A$= 60 MeV of the $Li$ isotopes. The $p + ^9 Li$ reaction is used as a reference case for the $^{11}Li$ calculations and the differences will allow to draw conclusions on the halo contributions. The theoretical results are compared to elastic scattering data of $^9Li + p$ at $E/A$= 60 MeV from ref. [6]. The data indicate a strong contribution from the halo structure of $^{11}Li$ on elastic scattering. In the measured angular range ($\sim 20^o - 60^o$ ) the elastic cross section for $^{11}Li + p$ is reduced to approximately $70\% - 30\%$ of the $^9Li + p$ cross section.

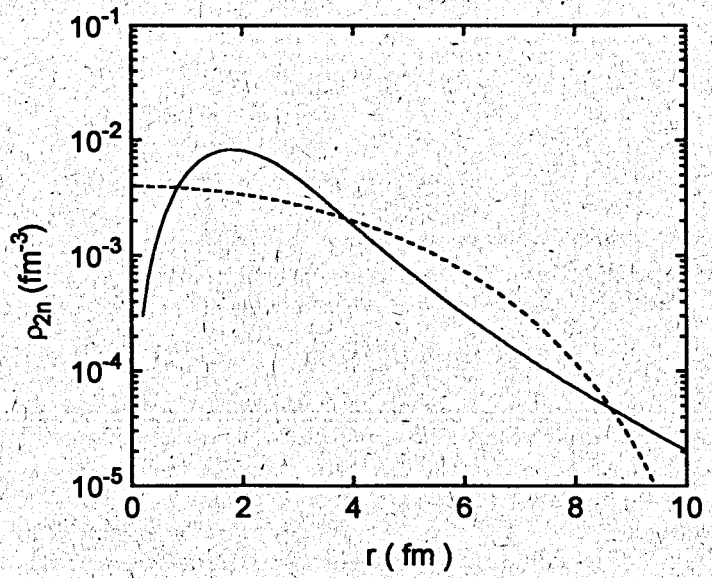


Fig. 1 Density distribution of halo neutrons in pairing [12] (solid line) and phenomenological (dashed line) [9] models of $^{11}Li$ nucleus.



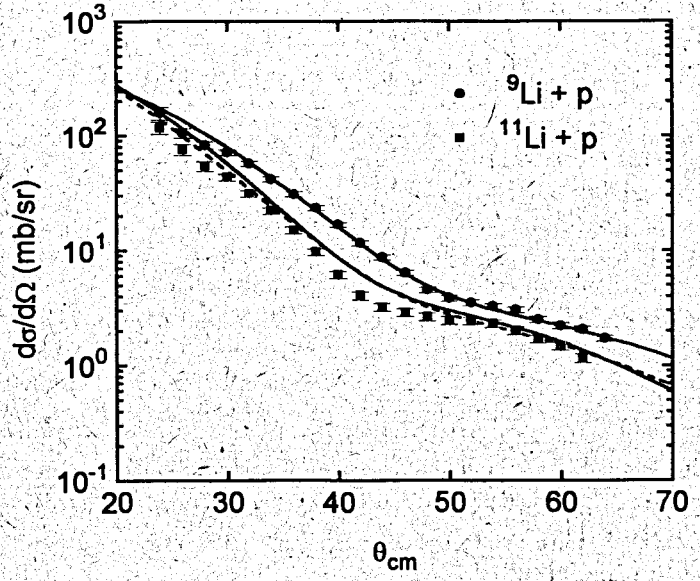


Fig. 2 Angular distributions for $^{11}Li+p$ and $^{9}Li+p$ elastic scattering as a function of c.m. angle. The experimental data for $^{9}Li+p$ at 60 MeV/A and $^{11}Li+p$ scattering at 62 MeV/A are indicated by dots and triangles, respectively. Solid and dashed lines are the results of calculations with microscopic pairing [12] and phenomenological [9] density models, respectively. The elastic angular distribution for $^{9}Li + p$ depicted by the upper curve (solid line) was obtained with the phenomenological optical potential of ref. [8].

The real and imaginary parts of the valence potentials have been determined by a folding calculation with the complex *NN* t-matrix of Franey and Love [10]. Knock-on exchange contributions were approximated by the pseudopotential approach. Calculations with an explicitly density dependent interaction gave almost indistinguishable results thus supporting the assumption that the tail part of the halo distribution is most important for elastic scattering. For $U_{core}$ the phenomenological $^9Li+p$ optical potential from [8] was taken. In the calculations including the polarization contributions $U_{val}^{pol} = U_{2n}^{pol}$ was obtained by solving Eq.(7) and Eq.(8) respectively, directly in coordinate space. In the strict sense of the impulse approximation, Eq.(7) should be considered in momemtum space but the differences to the present calculation are insignificant.

In order to study the sensitivity of elastic scattering on nuclear structure details different models for the halo neutron density were used. Microscopic descriptions are provided by self-consisted shell-model calculations [11] in the framework of the theory of finite Fermi systems and a mean-field approach with pairing correlations [12, 13]. For comparison the calculations were repeated with the phenomenological density distribution derived in ref. [9] from a Fourier-Bessel analysis and constrained in the Glauber approach to fit the experimental reaction cross sections for $^{11}Li$. Both microscopic models gave very similar results which indicates that the same type of structure aspects are covered. Only the results obtained with the pairing approach [12, 13] will be discussed in the following. The halo model densities are shown in Fig. 1. In shape the phenomenological and the microscopic density differ significantly. Microscopically, the pair of halo neutrons is found predominantly in a $1p_{1/2}^2$ orbital with an occupation probability of 96% and $2s_{1/2}^2$ configurations are admixed by only 4%. Common to both densities is the long-tailed halo distribution extending much beyond the nuclear surface.

Results for $^{9,11}Li+p$ elastic cross sections are compared to data in Fig. 2. Despite the strongly different radial shapes the differences in the elastic cross sections are minor. This insensitivity of elastic cross sections to details of the correlations in neutron halo wave functions was found already in ref. [18]. In foreward direction elastic cross sections are mainly sensitive to low radial moments of the nuclear density. Since the rms-radii of the two densities are very close similar results for the elastic cross section have to be expected. Thus, the data do not allow to decide on a specific structure model.

The experimental data are reproduced qualitatively except the dip near 45°. Reaction cross sections of $\sigma_{reac}$ = 415 mb and 445 mb are obtained for calculations with pairing and phenomenological densities, respectively. In [6] the reaction cross section for $^{11}Li+p$ scattering was estimated to be 360-414 mb. For $^9Li+p$ an optical model analysis gave $\sigma_{reac}$ = 263 mb. The comparison shows that rescattering on the halo neutrons significantly increases absorption which agrees with expectations. Apparently, we obtain the right degree of absorption which sufficiently well reproduces the overall reduction of elastic scattering on halo nuclei.

The sensitivity of elastic scattering with respect to a specific reaction model



was investigated by comparing results of folding and Glauber calculations. As in refs.[8, 9] only the imaginary part of the valence potential was calculated by using the Glauber forward scattering approximation

$$U_{2n}^{(Gl)}(r) = -i\frac{\hbar\nu}{2}\sigma_{pn}\rho_{2n}(r) \qquad (9)$$

where $\nu$ is the velocity of the incident proton and $\sigma_{pn}$ = 120 mb is the experimental total neutron-proton cross section at $E_{pn}$ = 60 MeV. The phenomenological density (Fig. 3b) leads to cross sections which are almost indistinguishable for the two reaction models. With the microscopic density (Fig. 3a), however, the Glauber calculations result in a lower elastic cross section at angles in the dip region. Interestingly, these differences are closely related to the potential structure. In the microscopic folding calculations a peculiar interplay of refraction and absorption from the real and imaginary parts of $U_{2n}$ is found in the tail region of the halo. The additional attraction provided by $U_{2n}^{(re)}$ is compensated to a large extent by an increased absorption from $U_{2n}^{(im)}$. For the smooth phenomenological density the cancellation is almost complete. Since the Glauber valence potential is purely imaginary the refractive part is missing and a different angular dependence of the cross section is found.

The value of elastic cross section at dip region depend on a subtle balance between real and imaginary parts of optical potential. The calculations indicate a special sensitivity to the nuclear surface region at distances $\sim 2-4$ fm. This is just the region where also nuclear polarization effects should contribute most efficiently. In Fig.4 results of calculations using Eq.(7) and the microscopic valence density are shown. The strength of the polarization potential was fitted to the cross section data and the results of Fig.4 were obtained with $\beta = 0.15$ MeV$^{-1}$. This is in surprisingly good agreement with theoretical average level densities $\rho(\frac{1}{2}^+) = 0.14\ MeV^{-1}$ and $\rho(\frac{1}{2}^-) = 0.15\ MeV^{-1}$ for the valence $s_{1/2}$- and $p_{1/2}$-states found in the Gorkov-pairing calculations for $^{11}Li$.

The degree of improvement is clearly seen from a comparison to the elastic cross section without the polarization potential. Interestingly, the shape of the medium-corrected cross section is close to the Glauber result, Fig.4. The explanation is found from Fig.5 where the different contributions to the $^{11}Li+p$ optical potential are displayed. Beyond r $\simeq 1\ fm$ the magnitude of imaginary part of the bare valence potential becomes larger than the real part. As a consequence, the real part of $U_{val}^{(pol)}$, Eq.(7), becomes repulsive (it is evident from approximate expression Eq. (8)) and compensates to a large extent the attraction from the bare folding potential. The imaginary part of $U_{val}^{(pol)}$ is always negative and increases the reaction cross section by about 5% to $\sigma_{reac} = 436\ mb$.

Quantitatively, these results are in agreement with other theoretical estimates of dynamical polarization effects. In a study of the polarization potential from the break-up of $^{11}Li$ Yabana et al. [19] found also an overall reduction of the elastic cross section in $^{11}Li+^{12}C$ scattering. Since the t-matrix corresponds to a complete

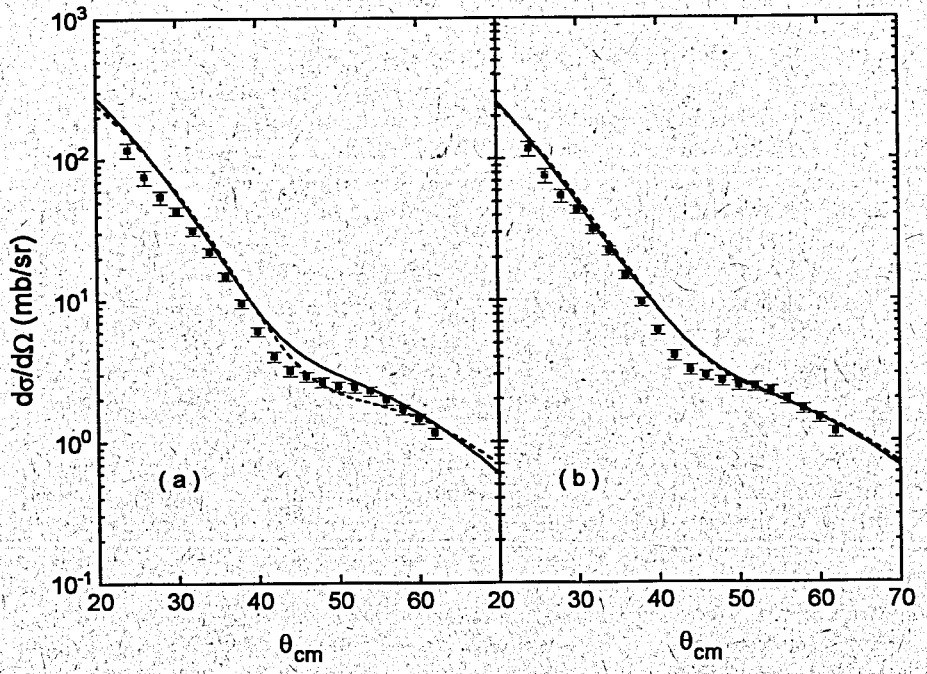


Fig. 3 Elastic scattering of $^{11}Li$ on a proton at 62 MeV/A for a) pairing [12] and b) phenomenological [9] halo density distributions. Results of t-matrix and the Glauber model calculations are indicated by solid and dashed lines, respectively.



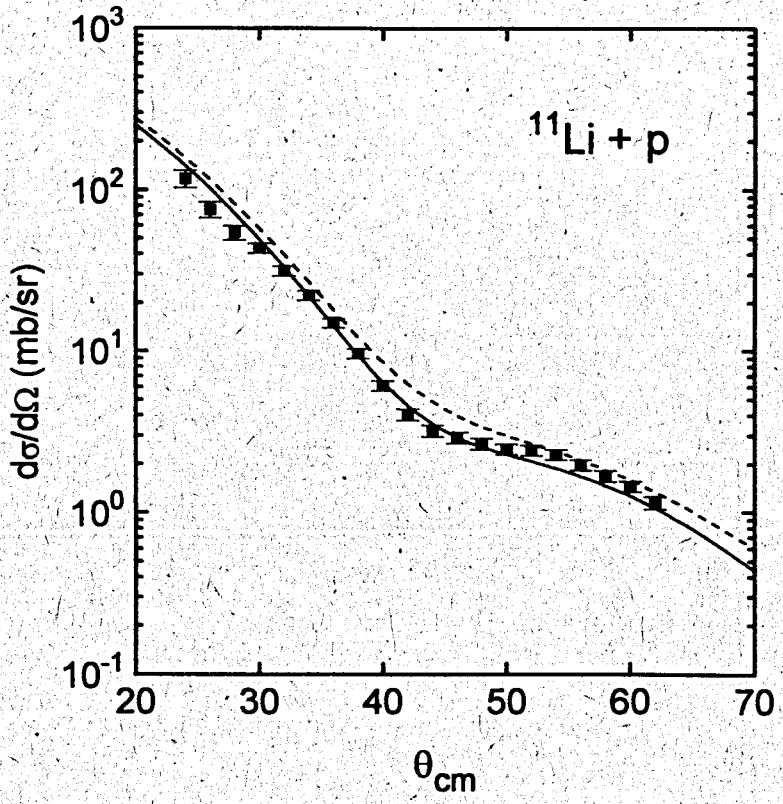


Fig. 4 Elastic scattering of $^{11}Li$ on a proton for the pairing density distribution with (solid line) and without (dashed line) polarization potential $U_{2n}^{(pol)}$.

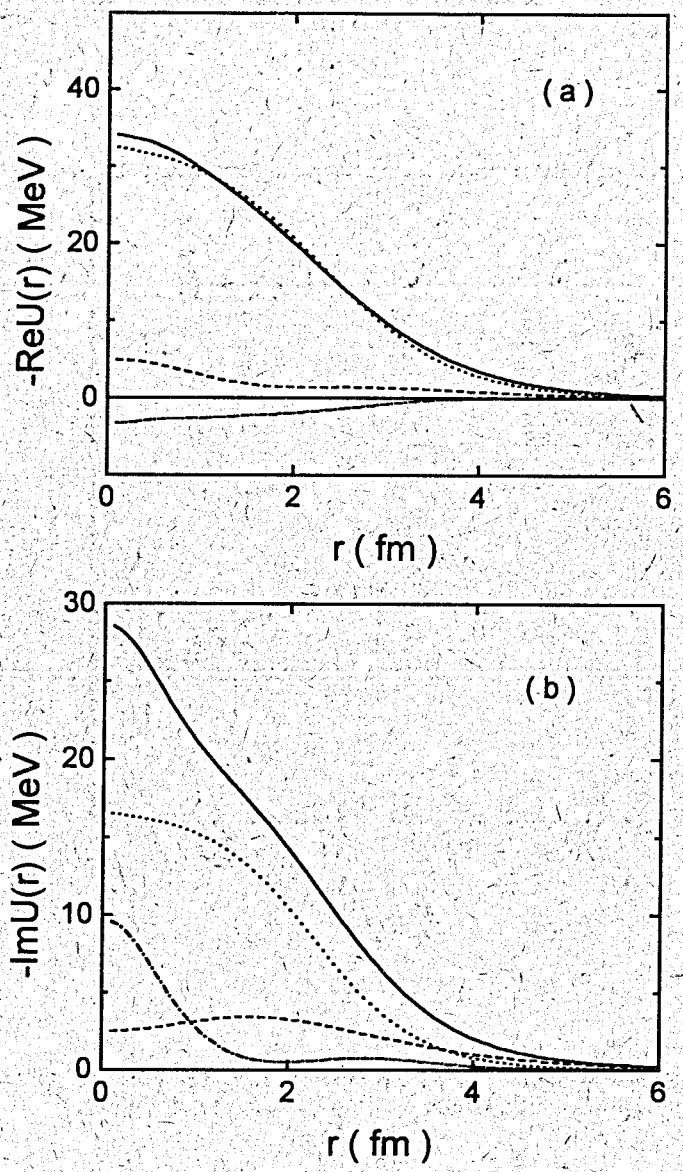


Fig. 5 Real (a) and imaginary (b) parts of optical potential as function of radius. Solid and dotted lines are total potentials for $^{11}Li$ and $^{9}Li$, correspondingly. Dashed and dashed- dotted lines are $U_{2n}$ and $\Delta U_{2n}$ potentials.



summation of the interactions between of pair of nucleons in a continuum also a part of break-up channels are included effectively but their contributions are hidden in the full scattering series and cannot be estimated separately. In ref.[4] it was found that the appearance of a proton halo in $^{8}B$ is strongly depending on dynamical polarizations of RPA-type. A common feature of these cases is the important role of intermediate couplings to unbound configurations.

## 4 Summary

A model for elastic nucleon scattering on halo nuclei was presented. The specific structure of dripline nuclei – given by a tightly bound core to which loosely bound valence particles are weakly coupled – justifies to treat the core and valence projectile–target interactions separately. The interaction with the core subsystem was described by a phenomenological optical potential taken from elastic proton scattering on a free nucleus. The interaction of the incident nucleon with the halo particles was derived in a microscopic folding model. The weak binding of the valence particles should allow to use the free space $NN$ t–matrix. An approximate treatment of corrections due to the peculiar level structure of dripline nuclei was proposed. The strong increase in the reaction cross section for $^{11}Li + p$ was already obtained by using the free t–matrix. The polarization potentials were found to reduce refractive scattering by peculiar cancellations. They generally tend to increase absorption and thus reduce the elastic cross section. More systematic investigations are clearly necessary before final conclusions can be drawn. But the present results indicate a strong evidence for the importance of polarization effects in dripline nuclei which is in agreement with expectations.

This work were supported by the Heisenberg-Landau program and Russian Fond for Fundamental Investigations ($N^{0}94 - 02 - 04619 - a$).

## References

[1] I. Tanihata et al., Phys. Rev. Lett., **55** (1985) 2676.

[2] T. Kobayashi et al., Phys. Rev. Lett., **60** (1988) 2599.

[3] J.J. Kolata et al., Phys. Rev. Lett., **69** (1992) 2631.

[4] W. Schwab, H. Lenske, H. Geissel et al., Z.Phys., **A350** (1995) 283.

[5] M. Lewitowicz et al., Nucl. Phys., **A562** (1993) 301.

[6] C.B. Moon et al., Phys. Lett., **B297** (1992) 39.

[7] A.A. Korsheninnikov et al., Phys. Lett., **B316** (1993) 38.

[8] S. Hirenzaki, H. Toki and I. Tanihata, Nucl., Phys., **A552** (1993) 57.

[9] A.K. Chaudhuri, Phys. Rev., **C49** (1993) 1603.

[10] M.A. Franey and W.G. Love, Phys. Rev., **C31** (1985) 488.

[11] S.A. Fayans; Phys. Lett., **B267** (1991) 357.

[12] H. Lenske, Proc. Int. Symp. on Structure and Reactions with Unstable Nuclei, Niigata 1991, eds. K. Ikeda, Y. Suzuki, World Scientific, Singapore, 1991; Proc. $7^th$ Int. Conf. on Nuclear Reaction Dynamics, ed. E. Gadioli, Ric.Sci. Suppl. N.100, Milano, 1994.

[13] H.G. Bohlen, H. Lenske et al., Z. Phys. **A 343** (1992) 489; Z. Phys. **A 344** (1993) 381.

[14] A.L. Fetter and J.D. Walecka, Quantum Theory of Many-Particle Systems, (McGraw-Hill, New York, 1971). 1969.

[15] F.J. Eckle, H. Lenske et al., Phys. Rev **C 39** (1989) 1662; Nucl. Phys **A 506** (1990) 159.

[16] V. Soloviev, Progr.Part.Nucl.Phys. **19** (1987) 107.

[17] C. Mahaux, R. Sartor, Nucl.Phys. **A 475** (1987) 247.

[18] F.A. Gareev et al., Europhys. Lett., **20** (1992) 487.

[19] K. Yabana, Y. Ogawa and Y. Suzuki, Phys. Rev., **C45** (1992) 2909.

[20] A.K. Kerman, H. McManus and R.M. Thaler, Ann. Phys., **8** (1959) 551.